MEASUREMENT OF $f(\alpha)$ FROM SCALING OF HISTOGRAMS, AND APPLICATIONS TO DYNAMICAL SYSTEMS AND FULLY DEVELOPED TURBULENCE

Charles MENEVEAU and K.R. SREENIVASAN

Mason Laboratory, Yale University, New Haven, CT 06520, USA

A procedure for obtaining $f(\alpha)$ directly from the scaling of histograms of multifractal measures is presented, and is applied to several measures arising in dynamical systems and fully developed turbulence. The method works well when the scaling range is large, and useful statistical information on iso-α sets such as lacunarity can be obtained. However, if the available scaling range is small, corrections of second order become importance and bias the $f(\alpha)$ curve obtained directly.

Multifractal measures can be characterized [1,2] by the so-called "generalized dimensions" D_q (recently identified with a critical dimension [3]), or by the $f(\alpha)$ distribution, the two being related via a Legendre transform [4,5]. In most cases, $f(\alpha)$ can be identified with a fractal dimension [4,5], and has been used for characterizing multifractal measures in a variety of applications, such as dynamical systems [5], onset of chaos in fluid flows [6,7], developing and fully developed turbulence [1,4,8–13], growth models [14], and random resistor networks [15]. Typically, if p is the measure in a box of size r, the scaling of the qth "cumulant" of p with the box size r involves the exponents D_q according to

$$\sum p^q \sim (r/L)^{(q-1)D_q}, \tag{1}$$

L being some outer length scale of the problem. Alternatively, one can define [16] a Hölder exponent α as a measure of the local singularity strength by

$$p \sim (r/L)^\alpha. \tag{2}$$

In addition, since the set of points where α has values within a band $d\alpha$ around α is assumed to have a fractal dimension $f(\alpha)$ [4,5], one can write that the number of boxes of size r that contain values of α in that range scale according to

$$N_r(\alpha) \sim \rho(\alpha)(r/L)^{-f(\alpha)} d\alpha. \tag{3}$$

The two sets of exponents $(\alpha, f(\alpha))$ and (q, D_q) are related by

$$\alpha = \frac{d}{dq}[(q-1)D_q], \tag{4a}$$

$$f(\alpha) = q\alpha - (q-1)D_q. \tag{4b}$$

Recently [9–11] these ideas have been applied to describe the field of turbulent energy dissipation in physical space; there p is identified with the fraction of turbulent energy dissipation contained in a box of size r. Then $f(\alpha)$ denotes the fractal dimension of the iso-α set of the dissipation field. Assuming that the distribution in physical space of the turbulent energy dissipation rate ϵ is related to the near-singularities of the Navier–Stokes equations, or to the singularities of the Euler equations modified benignly by viscosity [11,16], one might say that α is the strength of these singularities, with $f(\alpha)$ describing their measure. A similar description has been used for the dissipation of passive scalar fluctuations [12,13].

A question that arises when analyzing experimental or numerical data is whether to obtain $f(\alpha)$ by directly measuring the scaling exponents α and $f(\alpha)$, or indirectly by using an intermediate step requiring the determination of the exponents D_q. The $f(\alpha)$ curve in the latter case is obtained via the transformations (4a), (4b). We feel that this question de-

serves some elaboration in view of the fact that the intermediate step involving D_q's is usually justified by merely stating that they "smooth" the data [6]. Such smoothing effects may have unknown consequences [3] and deserve careful analysis.

The idea of measuring α and $f(\alpha)$ using eqs. (2) and (3) directly as equalities (therefore: $\alpha = \log_{r/L}(p)$ and $f(\alpha) = -\log_{r/L}[\rho(\alpha)N(\alpha)\mathrm{d}\alpha]$) has been used on several occasions [17,18]. In a recent paper, Arneodo et al. [19] covered the Hénon attractor with boxes of three different sizes and fitted numerically pre-exponential constants in eqs. (2) and (3) (with the assumption that they are independent of α) in order obtain the $f(\alpha)$ curve. These methods present difficulties when analyzing experimental or numerical data where cut-offs terminate the power-laws at length-scales that are not necessarily known a priori, when there are oscillations around power-laws [20], or when the pre-exponential terms depend on α.

In this note we briefly present a method for measuring $f(\alpha)$ directly that does not suffer from the problems mentioned above, and that is therefore applicable in principle for analyzing experimental or numerical data.

In order to extract $f(\alpha)$ directly from a multi-fractal measure using the box-counting algorithm, the measure is divided into disjoint boxes of size r_k. The procedure outlined below will be repeated for n_r different box-sizes, and therefore the box-size r_k is indexed with $k = 1, 2, ..., n_r$. Now one defines the quantity X as the logarithm of the total measure p contained in each box,

$$X = \log(p) ,\tag{5}$$

which varies from box to box. For a given box size r_k, let X assume values that fluctuate between $X_{\min}(r_k)$ and $X_{\max}(r_k)$. It is easy to see that if one plots the different values of $X_{\max}$ as a function of $\log(r_k/L)$, the slope of the graph will correspond to $\alpha_{\min}$. Similarly, the slope of $X_{\min}$ versus $\log(r_k/L)$ corresponds to $\alpha_{\max}$. In order to obtain intermediate values of α, the interval $[X_{\min}, X_{\max}]$ is discretized into n pieces of equal length ΔX (each segment is labeled with an integer index $i = 1, 2, ..., n$, as well as with the index k which indicates the size of the box-size r_k). Accordingly, plots of $X_{i,k}$ versus $\log(r_k/L)$ (these plots consisting of n_r points with $k = 1, 2, ..., n_r$) will

yield slopes α_i which are intermediate between $\alpha_{\min}$ and $\alpha_{\max}$.

In order to obtain the exponent $f(\alpha_i)$ one constructs raw histograms of the different values of $X_{i,k}$. Suppose that one measures $N(X_{i,k})\Delta X$, which is the number of boxes of size r_k such that the variable X takes on a value in the interval ΔX around $X_{i,k}$. The relation between $N(X)$ and $N(\alpha)$ is

$$N(\alpha) = -\frac{\mathrm{d}X}{\mathrm{d}\alpha}N(X) ,\tag{6}$$

where the negative sign appears because X is a decreasing function of α. For a fixed value of $\Delta\alpha$, one sees that $N(\alpha)$ is proportional to $N(X)\,\Delta X$. If eq. (3) is correct, the slope of graphs of $\log[N(X_{i,k})\,\Delta X]$ versus $\log(r_k)$ should be $-f(\alpha_i)$. Again, these graphs consist of n_r points for $k = 1, 2, ..., n_r$. However, when doing so, the values of $f(\alpha)$ systematically exceed the theoretically known $f(\alpha)$ (by as much as 10% for measures having a scaling range of about 4 decades), converging only very slowly to the asymptotic $f(\alpha)$ curve. The discrepancy can be explained by analyzing more carefully the ansatz (3). As recognized by van de Water and Schram [21], the normalization of the total measure requires that

$$\int C\rho(\alpha)(r/L)^{\alpha - f(\alpha)}\,\mathrm{d}\alpha = 1 ,\tag{7}$$

where C is a normalization constant that does not depend on α. The use of Laplace's method (special case of the steepest descent method) to evaluate this integral in the limit of small r/L at the dominant term (say at $\alpha = \alpha_1$) gives

$$CC_0(\alpha_1)[\ln(L/r)]^{-1/2}$$
$$\times \{1 - C_1(\alpha_1)[\ln(L/r)]^{-1} + ...\}$$
$$\times (r/L)^{\alpha_1 - f(\alpha_1)} = 1 .\tag{8}$$

where the coefficients $C_0(\alpha_1)$ and $C_1(\alpha_1)$ depend on the functions $\rho(\alpha), f(\alpha)$ and some of their higher derivatives evaluated at α_1. Since $\alpha_1 = f(\alpha_1)$, we can obtain C as a function of $\ln(L/r)$ and α_1 from eq. (8). Therefore, the prefactor in eq. (3) has to depend on $\ln(L/r)$, and eq. (3) should be rewritten as

$$N(\alpha)\,\mathrm{d}\alpha \sim [\ln(L/r)]^{1/2}$$
$$\times \{1 + C_1(\alpha_1)[\ln(L/r)]^{-1} + ..\}$$
$$\times (r/L)^{-f(\alpha)}\,\mathrm{d}\alpha .\tag{9}$$

In this way, the prefactors depending on $\ln(L/r)$ get cancelled when performing the integration that normalizes the measure, and the term in $[\ln(L/r)]^{1/2}$ cancels when performing the integration that leads to the Legendre transforms (4). For sufficiently small values of r/L, one can neglect higher order terms in eq. (9) and write for small ΔX that

$$N(X)|\Delta X| = N(\alpha)\,\Delta\alpha$$
$$\sim [\ln(L/r)]^{1/2}(r/L)^{-f(\alpha)}\,\Delta\alpha .\tag{10}$$

In view of this, one may now argue that $f(\alpha)$ should be measured from plots of $\log\{N(X)\Delta X \times [\ln(L/r)]^{-1/2}\}$ versus $\log(r/L)$. Note however that the outer cut-off L now enters the expression for $N(\alpha)\mathrm{d}\alpha$ in such a way that it is no longer a simple multiplicative prefactor, and it does affect the slope of the log–log plots. Since one does not necessarily know the exact value of L a priori, one needs an additional expression for the prefactor $\ln(L/r)$. From eqs. (2) and (5) it follows that

$$\Delta X/\Delta\alpha = \log(r/L) ,\tag{11}$$

meaning that $|\Delta X|$ is proportional to $\ln(L/r)$ for a fixed value of $\Delta\alpha$. Since ΔX is measured while obtaining the histograms, one can use the fact that the correction factor, from (10) and (11), is proportional to $|\Delta X|^{1/2}$. The measured number of occurrences $N(X)\Delta X$ can now be divided by $\Delta X^{1/2}$, and we conclude that graphs of $\log[N(X_{i,k})\Delta X^{1/2}]$ versus $\log(r_k/L)$ will yield a slope of $-f(\alpha_i)$.

Another problem in directly measuring $f(\alpha)$ is the sensitivity of the histograms on the positioning of boxes in the box-counting procedure. For measures on the line, one can start placing boxes at, say, x_0. One can start at some $x_0 \geq 0$, the first box being at $[x_0, r_k)$, the second at $[x_0 + r_k, x_0 + 2r_k)$, etc. It is useful to average $N_{i,k}$ over several such realizations (each corresponding to a specific x_0) of the box-counting; this eliminates the dependence on the positioning of the boxes [#1].

To illustrate the points made above, we study the binomial measure on the unit interval $[0, 1]$, with the parameters $l_1 = l_2 = 0.5$ and $p_1 = 1 - p_2 = 0.6$. The measure is constructed by iterating the multiplicative process 2^{17} times, and the unit interval is there-

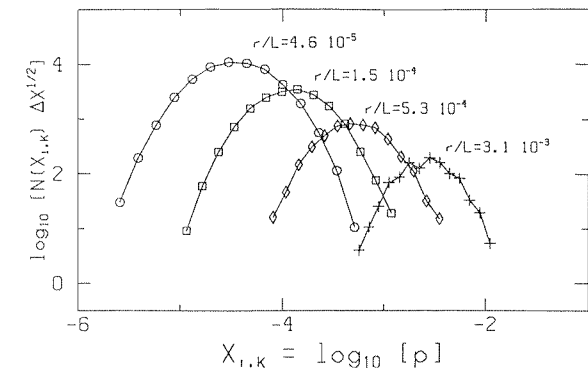[#1] This was suggested by Professor R.V. Jensen.

Fig. 1. Histograms of X for the binomial measure with parameters $p_1 = 1 - p_2 = 0.6$, corresponding to 4 different box-sizes. The histograms are averages over 50 realizations of random positioning of the boxes (see text), and include the correction $\Delta X^{-1/2}$.

fore divided into 2^{17} pieces of length 2^{-17}. We use 20 different sizes for r_k and the range of values of X (or α) is divided into 14 pieces, i.e., $n_r = 20$ and $n = 14$. The boxes are deliberately chosen to be different from the natural sizes 2^{-m}, in order to simulate the situation that arises when analyzing experimental or numerical measures where the natural partition, if it exists, is unknown. Also, averaging of $X_{i,k}$ and $N_{i,k}$ over 50 different starting positions x_0, placed randomly in the interval $[0, 10^{-2}]$ is performed.

Fig. 1 shows the histograms for 4 different values of the box-size. Fig. 2 shows plots of $X_{i,k}$ versus $\log(r_k/L)$ for 6 different values of $i = 1, 3, 6, 8, 11$ and 14 along with least-square linear fits. By measuring the slopes of such curves one obtains 14 values of α ranging from 0.74 ± 0.005 to 1.30 ± 0.01, values that agree well with the theoretical extremes of the curve, namely $\log_2 p_1^{-1}$ and $\log_2 p_2^{-1}$. Figs. 3a–3f shows plots of $\log(N_{i,k}\Delta X^{1/2})$ versus $\log(r_k/L)$ for the same values as before, along with the least-square linear fits. The slopes of these graphs correspond to $-f(\alpha_i)$.

We are interested in quantifying deviations from perfect power-laws, a subject that has received attention recently. The deviations occur as oscillations around power-laws [20], or lacunarity [16]. Since they are not the central point here, we will for simplicity represent these deviations as uncertainty in the slope of the line that one is fitting (and as "error bars" on the exponent). Essentially, these "error bars" are computed as the ratio between the stan-
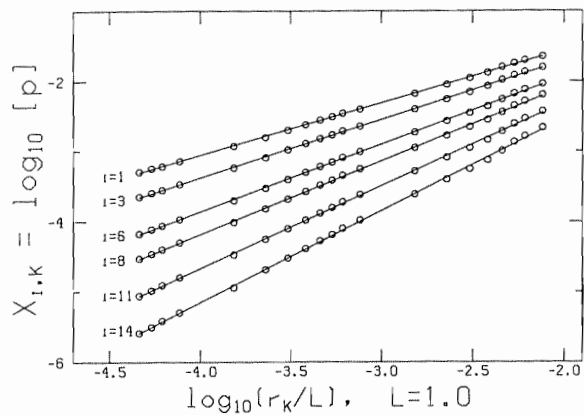
Fig. 2. Scaling of the histogram elements $X_{i,k}$ with respect to the box-size r_k. Plotted are 6 different sets of values of $X_{i,k}$ for $i=1,3,6,8,11$ and 14 as applied to the binomial measure described in the text. The slope of the different lines correspond to the values of α_i.

dard deviation of the data around the power law, divided by the scaling range. It should be kept in mind that such oscillations are real for "lacunar fractals" and contain additional information; as such they do not really constitute an error. The present representation is used only for brevity and convenient comparison of the different methods of obtaining $f(\alpha)$.

The results of α and $f(\alpha)$ obtained by the present method can be compared with the usual method of measuring the exponents D_q and then applying the Legendre transforms (4). To obtain the D_q's, the measure is divided again into boxes of size r_k, and graphs of $\log(\sum p^q)^{1/(q-1)}$ versus $\log(r_k/L)$ are plotted; according to eq. (1), these plots would have a slope equal to D_q. This procedure is repeated for 29 different values of q between -9 and $+9$. Also, the choice of values for the box-sizes r_k is exactly the same when measuring D_q as when measuring α and $f(\alpha)$

directly. Once the D_q's are known, each with its corresponding "error" σ_{D_q}, we contruct two more D_q curves, $D_q^+ = D_q + \sigma_{D_q}$ and $D_q^- = D_q - \sigma_{D_q}$. The Legendre transforms (4) are applied to the three curves using centered differences on the 29 values of q. One then obtains three $f(\alpha)$ curves, one of them representing the result using the mean D_q curve, and the other two representing the error incurred in the calculation of $f(\alpha)$ due to the "errors" σ_{D_q} in measuring D_q.

Fig. 4 shows $f(\alpha)$ obtained for this measure using different procedures. The continuous line in fig. 4 corresponds to the theoretical prediction obtained using eqs. (2.31) and (2.33) of ref. [5]. The diamonds represent $f(\alpha)$ obtained from D_q and both dashed lines were obtained from $D_q^\pm$. The squares in fig. 4 correspond to the direct determination of α and $f(\alpha)$ from plots such as figs. 2 and 3, according to the procedure described here. It can be seen that the agreement between all procedures is generally good. It is important to point out that the errors incurred by the present method of scaling of histograms (with the averaging over the positioning of the boxes as described earlier) does not appear to be any worse than in the usual method via D_q. Also, the discrete points on fig. 4 have to be interpreted as an approximation to $f(\alpha)$; better approximations can be obtained by increasing n.

As an example from dynamical systems, we con-

sider the period-doubling attractor at the accumulation point of the logistic map

$$x_{n+1} = \lambda_\infty(1-2x_n^2) . \qquad (12)$$

The map is iterated 2^{22} times with λ_∞ approximated by λ_{22} (the parameter that generates a 2^{22} period), the interval $[-1, 1]$ is divided into 10^6 pieces in order to generate a discretized measure. Thirty-two values of r_k are used ($n_k = 32$). As before, $n = 14$. Fig. 5a shows $f(\alpha)$ of the attractor obtained by different methods. The continuous line is obtained by solving for the partition function following Halsey et al. [5]. The large "error bars" on $f(\alpha)$ and the large "error" incurred by the D_q method are due to the fact that the lacunarity of this measure is very pronounced, and the "scatter" in all appropriate log-log plots is therefore quite large. This leads to considerable "uncertainty" in the measurement of power-law exponents [19].

As another example from dynamical systems, we consider the measure formed by the critical trajectory of the standard circle map with golden mean winding number

$$\theta_{n+1} = \theta_n + \Omega - (2\pi)^{-1}\sin(2\pi\theta_n) \quad [\text{mod } 1] . \qquad (13)$$

The map is iterated with a bare winding number Ω equal to Ω_{27} (i.e. there is a periodic orbit corresponding to the 27th Fibonacci number). The map is iterated 3×10^7 times. Therefore, there are several periodic orbits, slightly biasing the results on the rarefied regions of the attractor, but the effects elsewhere are negligible. The unit interval is discretized
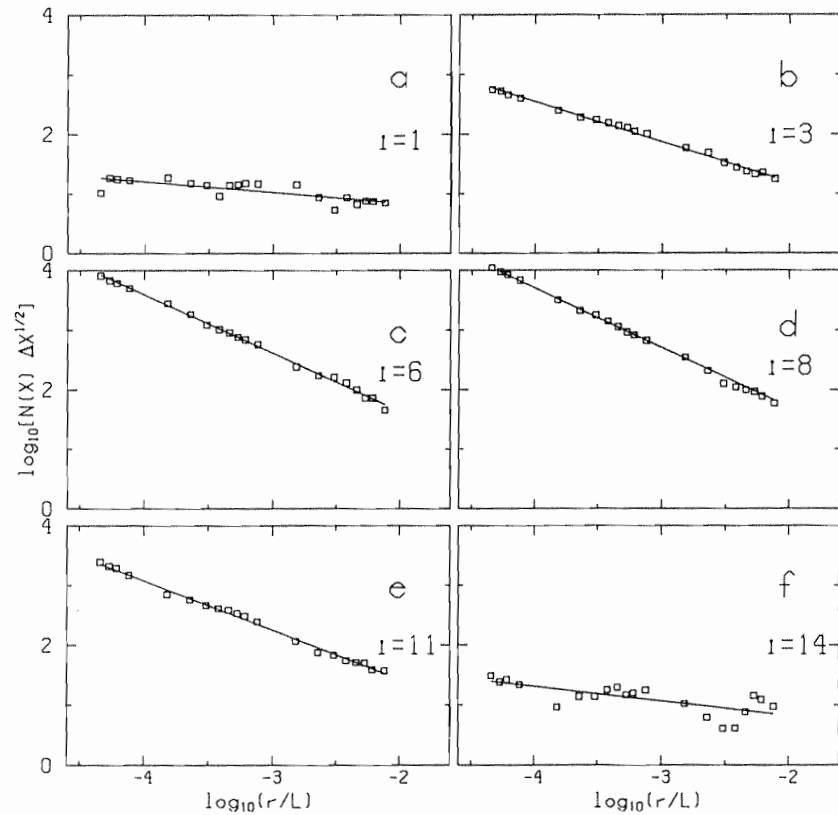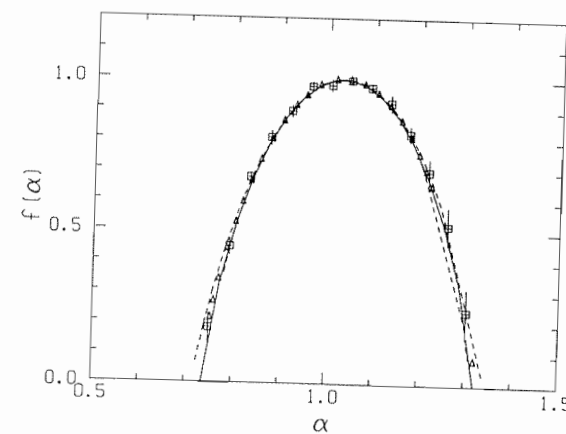

Fig. 3. Scaling of the number of occurrences of a given value of $X_{i,k}$ as applied to the binomial measure, including the logarithmic correction; averaging has been performed over 50 realizations, each of which corresponds to a random positioning of the boxes on the measure. The slope of the lines correspond to the values of $-f(\alpha_i)$.

Fig. 4. The $f(\alpha)$ curve for the binomial measure with $p_1 = 0.6$. Squares are obtained using the scaling of histograms (from figs. 2 and 3). Triangles are obtained using the D_q exponents, and dashed lines represent the uncertainty involved in that method (see text). The continuous line is the theoretical curve.
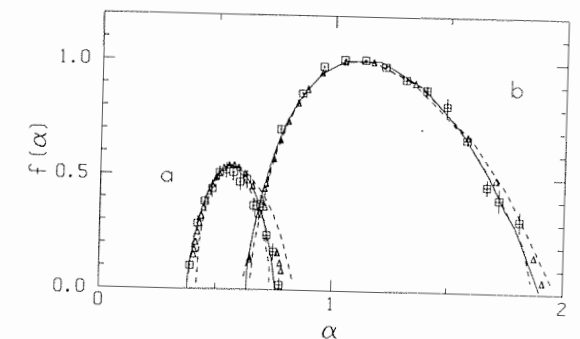

Fig. 5. (a) The $f(\alpha)$ curve of the attractor of the logistic map. Symbols as in fig. 4. The continuous line is obtained by numerically solving for the partition function. (b) The $f(\alpha)$ curve of the attractor of the circle map. The meaning of symbols and lines is the same as in (a).

into 10^5 pieces; by counting the number of iterations that fall into each piece, a measure is generated. Fig. 5b shows $f(\alpha)$ for the attractor obtained by the different methods. The continuous curve corresponds to the "theoretical" prediction (obtained again by solving numerically for the partition function, following ref. [5]). The agreement between the results obtained by using D_q and the scaling of histograms is good and the errors incurred in both methods are of the same order.

Finally, we apply the procedure of obtaining $f(\alpha)$ to one-dimensional cuts through the dissipation field of turbulent kinetic energy in fully developed turbulent flows. Here, the process of eddy-breakdown and cascade of kinetic energy to smaller scales can be thought of as a multiplicative process giving rise to a multifractal distribution of energy dissipation (see refs. [9,10], and early ideas [1,2]). We consider measurements in a constant pressure turbulent boundary layer on a flat plate at moderate Reynolds number and base the analysis on measured time series of the streamwise velocity component $u_1(t)$ using hot-wire anemometry. The free-stream velocity of the flow is 12 m/s, the boundary layer thickness δ at the measuring station is 4 cm, and the hot-wire is located at a height above the wall of $y/\delta = 0.2$. The hot-wire is operated at an overheat ratio of 1.7 and the signal is low-pass filtered (roll-off rate of 18 dB/octave) with a DANTEC 55D26 signal conditioner. The filter was set at 12.5 kHz (which is the noise floor observed in the on-line power spectra taken with an HP 3561A spectrum analyzer). The signal is digitized with 12 bit resolution on a MASSCOMP 5500 computer at a sampling rate of 25 kHz. Ten consecutive data files, each consisting of 10^6 points, are used for the analysis. This ensured stationarity of the computed statistical data. The Kolmogorov microscale η is 0.016 cm and the Taylor microscale λ is 0.3 cm. The Reynolds number based on λ is moderate ($R_\lambda = u'\lambda/\nu = 105$), the relatively short scaling range available (at most between one and two orders of magnitude) being especially suited for the present illustrative purposes.

As has been the practice, Taylor's hypothesis is used. That is, it assumed that the time series can be considered as a linear cut through the "frozen" turbulent velocity field in the streamwise direction (say x-axis). Furthermore, it is assumed that the square

of the gradient in only one direction is representative of the actual dissipation consisting of 9 terms, therefore $\epsilon \sim (\partial u_1/\partial t)^2$. These assumptions were shown to be satisfactory in a slightly different context in ref. [12]. The gradients are obtained by simple finite differences. (More elaborate methods of evaluating the derivatives were tested, and no difference on the resulting scaling exponents was observed.)

In order to measure $f(\alpha)$ of the dissipation field ϵ, p of eq. (5) is replaced by E_r, the total energy dissipation within a box of size r_k. Since multiplicative constants do not alter the power-laws, it is convenient to normalize E_r as

$$E_r = \int_r \epsilon \, dx \bigg/ \int \epsilon \, dx, \qquad (14)$$

where the integral in the numerator is performed within a segment of size r_k, and that in the denominator over the entire data set of 10^7 points ($\sim 4 \times 10^4 L$). Therefore $X = \log(E_r)$. We use 20 different box-sizes, ranging roughly from 10η to $5L$, and perform averaging over the box positions by selecting randomly 50 values of x_0.

A problem arises due to the entrainment of fluid from outside the boundary layer when it occasionally reaches the hot-wire in an irrotational state. One then observes extremely low values of dissipation, which produces very long tails on the left hand side of the histograms of E_r. This phenomenon has been observed before in two-dimensional slices of a turbulent jet [12]. Since this effect is irrelevant to the energy cascade, and (in any case) occurs extremely rarely at the measurement station, we eliminate such "laminar" regions from the data by setting an appropriate threshold and hold-time on the dissipation. This elimination procedure could bias the results on the low-intensity regions of the measure (right-most part of the $f(\alpha)$ curve), but it was verified that there is no influence on the rest of the curve when doing this. More details on this issue will be reported elsewhere [23].

Fig. 6 shows the resulting histograms for several values of the box-size. Here, instead of discretizing the histograms in equal pieces between X_{min} and X_{max}, the portion between X_{max} and the maximum of $N(X)$ is divided into 10 parts, and that between the maximum and X_{min} is divided into another 10 parts. This
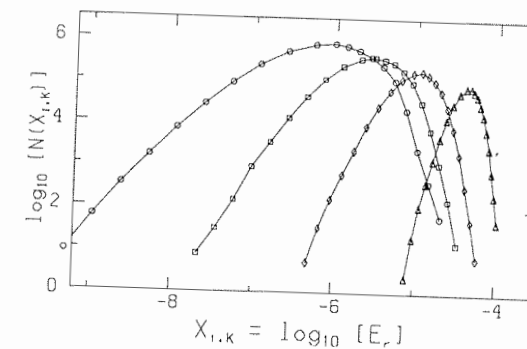
Fig. 6. Histograms of log (E_r) (without including the logarithmic correction) of linear intersections through the dissipation field ϵ in the laboratory boundary layer for different box sizes: $r/\eta = 20$ (circles), $r/\eta = 60$ (squares), $r/\eta = 200$ (diamonds), $r/\eta = 800$ (triangles).

is necessary because the curves become asymmetric for small box-sizes, with the left part becoming longer in comparison with the right.

Figs. 7 and 8 show plots whose slopes are α and $-f(\alpha)$. For small r, the behavior of the curves in fig. 7 is the same as those of ref. [9] in the D_q measurement: the results for the low intensity of dissipation are influenced by noise (digitizer and otherwise) and perhaps also by the undetected laminar regions interspersed in the turbulent ones. The straight lines are least-square fits to points in the range between 30η and 1000η for the high intensity regions ($i < 11$), and between 100η and 1000η for the low-intensity regions ($i \geqslant 11$). Oscillations are present in fig. 8, especially for low values of $f(\alpha)$. Their amplitude may be related to the lacunarity of iso-α sets, which increases near the tails of the $f(\alpha)$ curves for the sparser iso-α sets.
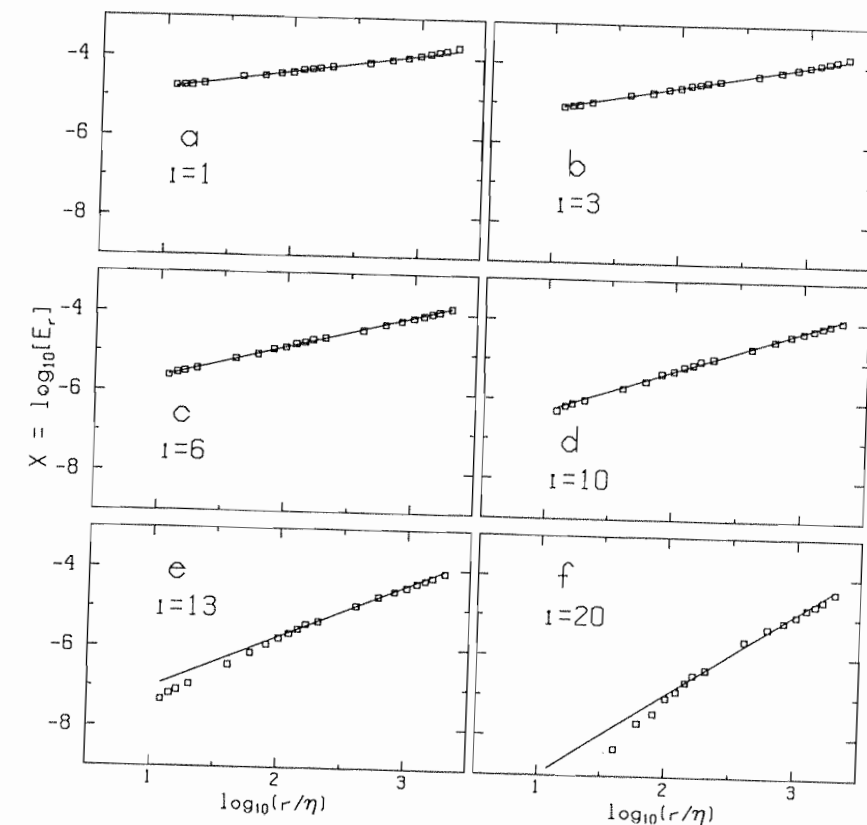

Fig. 7. The scaling of E_r with respect to the box-size r/η. The slope of the different lines corresponds to the values of α_i. The scaling range is larger for $i < 8$ (high intensity dissipation), but gets significantly worse for $i > 8$ (low intensity regions).
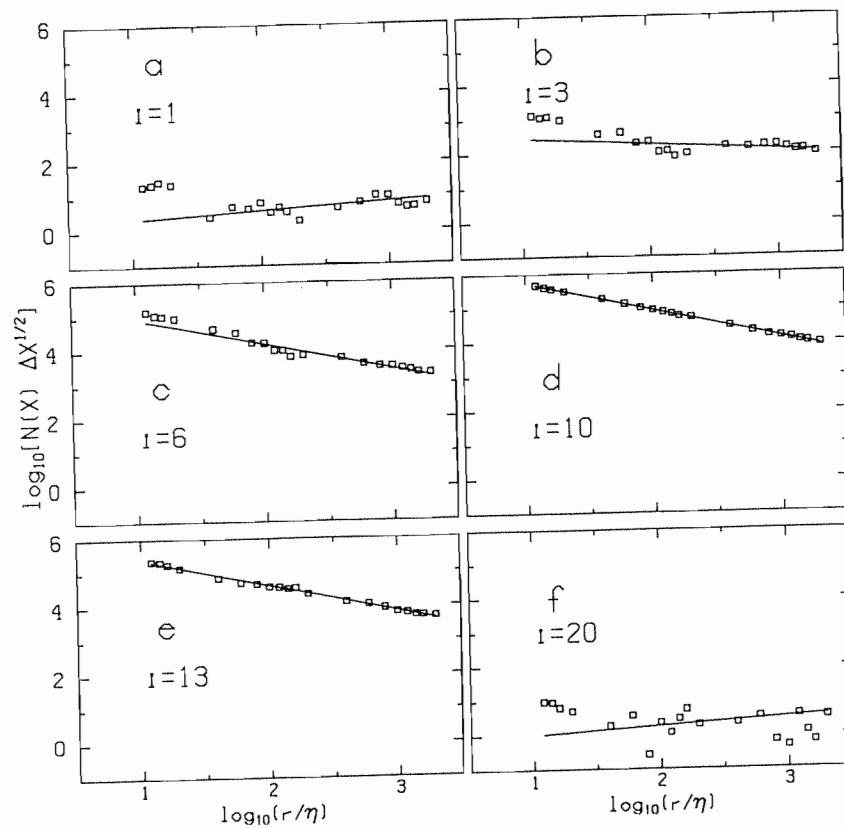
Fig. 8. The scaling of the number of occurrences of a given value of $X=\log(E_r)$, including the logarithmic correction and averaging over 50 realizations of random positioning of the boxes for the dissipation field. Strong oscillations can be seen corresponding to the extreme values of α, suggesting that these iso-α sets are highly lacunar.

The squares in fig. 9 show the resulting values of α and $f(\alpha)$. The continuous curve corresponds to the average result obtained by the D_q method using many data sets [9], each of length equal to about
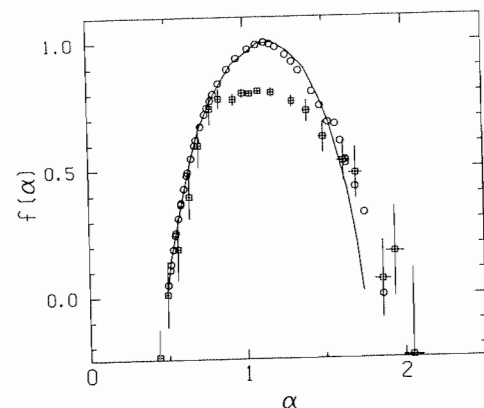
30L. The circles correspond to the D_q method using 10^7 point long data file contiguously. In the latter case, $\sum E_r^q$ is calculated using the histograms as

$$\sum E_r^q \sim \sum_{i=1}^{n} (10^{X_{i,k}})^q N(X_{i,k}) \,\Delta X,$$

◀ Fig. 9. The $f(\alpha)$ curve of one-dimensional sections through the dissipation field of fully developed turbulent flows. The continuous line corresponds to the $f(\alpha)$ curve obtained from the average D_q curve measured in a variety of fully turbulent flows (see ref. [9]) using many data of short length (about 30 integral scales for the laboratory flows). The circles correspond to the $f(\alpha)$ curve obtained from the D_q method applied to the very long data set in the boundary layer (see text). The squares correspond to the values of α and $f(\alpha)$ obtained by the direct method from the slopes in figs. 7 and 8. The significant discrepancy is due to the small scaling range available at the moderate Reynolds number in the boundary layer. Terms of order $[\ln(L/r)]^{-2}$ become important and bias $f(\alpha)$.

for q ranging from -4 to $+4$. (Note that the log–log plots used to obtain D_q from long-time averages, show less extensive linear regions than similar curves for shorter-time averages of ref. [9], but we prefer to relegate a detailed discussion to a later date [24].) The circles and the continuous curves agree reasonably well, except for the large α region where there is an overshoot in the long-time average results. This is due to the problems encountered in the low-intesity regions of the histograms, as explained before. In spite of this difference, it is clear that our earlier results [9] are generally confirmed; in particular, the $f(\alpha)$ curve for one-dimensional cuts through the dissipation field falls between $\alpha_{\min} \sim 0.5$ and $\alpha_{\max} \sim 1.75$, and $f(\alpha)_{\max}=1.0$.

In contrast, the directly obtained values of $f(\alpha)$ (squares) systematically fall below the expected curve by as much as 20% in the central portion. The explanation for this discrepancy lies in the fact that the scaling range of this experimental measure is very small (about one decade). In such a case, the higher order terms that were neglected in eq. (8) become important. Taking the derivative of the natural logarithm of eq. (8) with respect to $\ln(r/L)$, one obtains

$$\frac{\mathrm{d}\ln[N(\alpha)\,\mathrm{d}\alpha]}{\mathrm{d}\ln(r/L)}$$
$$= -f(\alpha) - [2\ln(L/r)]^{-1}$$
$$+ C_1(\alpha_1)[\ln(L/r)]^{-2} + \dots, \tag{15}$$

which would correspond to the slope of log–log plots if no finite scale-range corrections are made. The correction procedure for $\Delta X^{1/2}$ cancels the term of order $[\ln(L/r)]^{-1}$, but if L/r is not sufficiently large, $[\ln(L/r)]^{-2}$ cannot be neglected. Eq. (15) is another way of showing that we would correct for the first order term by knowing $\ln(L/r)$, but not for the second order term because $C_1(\alpha_1)$ is unknown. For one decade of scaling, $[\ln(L/r)]^{-2}$ is of the order 0.2 – evidently quite large.

These results illustrate that the method of obtaining $f(\alpha)$ through histograms works for measures with large scaling range, and that the values of $f(\alpha)$ resulting from the present method of scaling of histograms with logarithmic corrections have to be interpreted as an effective exponent accurate only up to order $[\ln(L/r)]^{-2}$. If we had not included the

correction $\Delta X^{1/2}$, the results would be accurate only up to order $[\ln(L/r)]^{-1}$ which, even for 10 decades of scaling, is about 5%. This explains the overshooting of $f(\alpha)_{\max}$ that was observed in ref. [18].

It should be noted that one can in principle increase the accuracy of the method to higher orders in $\ln(L/r)$ using the Richardson extrapolation. One essentially expands the function $g[\ln(L/r)] = \ln[N(X)\Delta X]$ in terms of $\ln(L/r)$, and uses the g's evaluated at different length scales to calculate constants such as $C_1(\alpha_1)$ in eq. (15). However, this is inaccurate in practice, since g is not always sufficiently smooth (see fig. 8). Yet another comment on fig. 9 relates to the few data points where $f(\alpha)$ is negative. That part of $f(\alpha)$ probably corresponds to "latent singularities" [3] that occur very rarely, detected by this method because it is based on very long samples. More details on both issues will be reported in the future [24]. It should be noted that we could not have detected these singularities had we used much less data although, for the present Reynolds number, 5×10^5 points or so would have reproduced the positive part of the curve quite adequately.

We conclude that if one includes the first order logarithmic correction, performs sufficient smoothing over different box positions, and has a scaling range that is sufficiently large, the present method of obtaining directly the $f(\alpha)$ curve is a useful alternative to the usual method via D_q. Furthermore, the histograms allow better insight into the statistics of α, and oscillations in log–log plots can give useful information on the lacunarity of iso-α sets. It must be stressed, however, that for measures possessing less than about 3 decades of scaling, the D_q method gives $f(\alpha)$ curves that converge much faster to the asymptotic results.

The procedure introduced in this note could have been implemented equally well using discrete probability densities instead of histograms (fraction of boxes instead of number of boxes). In that case, one measures $d-f(\alpha)$ instead of $-f(\alpha)$, d being the dimensionality of the embedding space. (The quantity $d-f(\alpha)$ is called $-\rho(\alpha)$ in ref. [3]). It is well known that box-counting methods are extremely time consuming when applied to measures embedded in spaces of dimension greater than 2. The alternative is to use correction exponents [8], return times [6], nearest neighbour distances [21,24], etc. General-

izing the present procedure involves expressing α in terms of these quantities and counting the occurrences of a given number of points falling in a ball of certain radius, range of return times, nearest neighbour distances, etc. This has to be repeated for varying length scales. The quantities α and $f(\alpha)$ can then be determined from the appropriate log–log plots. Recently [25,26], efforts have been made to determine $f(\alpha)$ directly using the notion of "crowding indices", without using regression (log–log) plots. We repeat that in experimental situations, where the status of power-laws is not necessarily clear, it is important to inspect the log–log plots. Finally, we point out that Chhabra and Jensen [27] have very recently proposed a method to measure α and $f(\alpha)$ directly as weighted averages over the distribution of α. This method has also been applied to turbulence [28], with satisfactory results.

References

[1] B.B. Mandelbrot, J. Fluid Mech. 62 (1974) 305.

[2] H.G.E. Hentschel and I. Procaccia, Physica D 8 (1983) 435.

[3] B.B. Mandelbrot, in: Fluctuations and pattern formation, eds. H.E. Stanley and N. Ostrowsky (1988), in print.

[4] U. Frisch and G. Parisi, in: Turbulence and predictability in geophysical fluid dynamics and climate dynamics, eds. M. Ghil, R. Benzi and G. Parisi (North-Holland, Amsterdam, 1985) p. 84.

[5] T.C. Halsey, M.H. Jensen, L.P. Kadanoff, I. Procaccia and B.I. Shraiman, Phys. Rev. A 33 (1986) 1141.

[6] M.H. Jensen, L.P. Kadanoff, A. Libchaber, I. Procaccia and J. Stavans, Phys. Rev. Lett. 55 (1985) 2798.

[7] D.J. Olinger and K.R. Sreenivasan, Phys. Rev. Lett. 60 (1988) 797.

[8] R. Benzi, G. Paladin, G. Parisi and A. Vulpiani, J. Phys. A 17 (1984) 3521.

[9] C. Meneveau and K.R. Sreenivasan, Nucl. Phys. B. Proc. Suppl. 2 (1987) 49.

[10] C. Meneveau and K.R. Sreenivasan, Phys. Rev. Lett. 58 (1987) 1242.

[11] K.R. Sreenivasan and C. Meneveau, Phys. Rev. A 38 (1988) 6287.

[12] R.R. Prasad, C. Meneveau and K.R. Sreenivasan, Phys. Rev. Lett. 61 (1988) 47.

[13] R. Ramshankar, The dynamics of countercurrent mixing layers, Ph.D. thesis, Yale University (May 1988).

[14] P. Meakin, A. Coniglio, H.E. Stanley and T. Witten, Phys. Rev. A 34 (1986) 3325.

[15] L. de Arcangelis, S. Redner and A. Coniglio, Phys. Rev. B 34 (1986) 4656.

[16] B.B. Mandelbrot The fractal geometry of nature (Freeman, San Francisco, 1982).

[17] K.J. Måløy, F. Boger, J. Feder and T. Jøssang, in: Time dpendent effects in disordered materials, eds. R. Pynn and T. Riste (Plenum, New York, 1987) p. 111.

[18] M.C. Gutzwiller and B.B. Mandelbrot, Phys. Rev. Lett. 60 (1988) 673.

[19] A. Arneodo, G. Grasseau and E.J. Kostelich, Phys. Lett. A 124 (1987) 424.

[20] R. Badii and A. Politi, Phys. Lett. A 104 (1984) 303;
L.A. Smith, J.D. Fournier and E.A. Spiegel, Phys. Lett. A 114 (1986) 465.

[21] W. van de Water and P. Schram, Phys. Rev. A 37 (1988) 3118.

[22] R. Kraichnan, J. Fluid Mech. 62 (1974) 305.

[23] C. Meneveau, The multifractal nature of turbulence, PhD. thesis, Yale University (May 1989).

[24] R. Badii and A. Politi, J. Stat. Phys. 40 (1985) 725.

[25] P. Grassberger, R. Badii and A. Politi, J. Stat. Phys. 51 (1988) 135.

[26] R. Badii and G. Broggi, Phys. Lett. A 131 (1988) 339.

[27] A. Chhabra and R.V. Jensen, Phys. Rev. Lett. (1989), to be published.

[28] A. Chhabra, C. Meneveau, R.V. Jensen and K.R. Sreenivasan, in preparation.